Yard truck retrofitting and deployment for hazardous material transportation in green ports

Qian Zhang [a], Shuaian Wang [b], Lu Zhen [a,*]

[a] *School of Management, Shanghai University, Shanghai, China*
[b] *Department of Logistics & Maritime Studies, The Hong Kong Polytechnic University, Kowloon, Hong Kong*

Abstract: In the design of green ports, the strategic decision on what types of container transportation equipment are appropriate is extremely important. Yard trucks (YTs) are indispensable in container transportation. In this paper, we propose a YT retrofitting and deployment problem that considers hazardous material transportation in green ports. A stochastic mixed-integer programming model is developed to minimize the costs of purchasing, retrofitting, and chartering YTs and the operation costs during the planning horizon. An enhanced Benders decomposition based on a Lagrangian relaxation algorithm is developed to solve the model. We conduct numerical experiments to verify the effectiveness of the proposed algorithms. We find that the larger free carbon emission quotas provided to enterprises by the government are not always an optimum solution. This research also provides suggestions that can inform decisions about YT retrofitting and deployment and that can contribute to the sustainable development of green ports.

Keywords: Green ports; yard truck retrofitting and deployment; stochastic programming; enhanced Benders decomposition based on Lagrangian relaxation.

1.Introduction

Over 85% of global trade is transported by the shipping industry, and the green development of the shipping industry and the limitation of its greenhouse gas (GHG) emissions are important international policy concerns (UNCTAD, 2018, 2020). According to a report by the International Maritime Organization (IMO), nearly 240 million tons of marine fuel are consumed through shipping activities every year. GHG emissions, including carbon dioxide and methane, increased from 977 million tons in 2012 to 1076 million tons in 2018, with a 9.6% growth rate (IMO, 2021). GHG emissions pose a significant problem for the natural environment as they can cause extreme weather and natural disasters, which threaten human economic and social development. Some authorities have made a lot of efforts to control the carbon emissions in the ports (Wang et al., 2021), for example, the IMO proposes to impose a long-term carbon emission tax, which indicates that constructing environmentally

* Corresponding author.

E-mail addresses: qianzhang@shu.edu.cn (Q. Zhang), wangshuaian@gmail.com (S. Wang), lzhen@shu.edu.cn (L. Zhen).

friendly green ports has recently become the main priority to effectively control emissions over the long term (Wang et al., 2018).

The loading, unloading, and transportation of containers in ports produce a high volume of air emissions, to prevent the spread and escalation of GHG emissions, the construction of green ports came into the scene. A green port refers to a sustainable port that makes efficient use of resources, reduces energy consumption and pollution, has a scientific and reasonable layout, and obtains good economic benefits. The application of green technology and infrastructure is a positive response to environmental changes for sustainable development and can provide competitive advantages (Kaluarachchi, 2021). The technical retrofitting of port loading/unloading and transportation equipment, the optimization of port layouts, and the use of renewable low-carbon and carbon-neutral energy (such as solar photovoltaic systems or hydropower) are essential for improving the environmental impacts of port operations (Jin et al., 2018; Zhou et al., 2021; Qin et al., 2021). Many seaports (such as Shanghai port and Rotterdam port) have installed fully electrified equipment. The utilization of such equipment can contribute to tackling climate change (Iris & Lam, 2021).

Hazardous cargo such as flammable, explosive, or toxic materials are commonly handled in ports and are typically stored in the same areas or adjacent to non-hazardous materials (Hervas-Peralta et al., 2020). Accidents in operations involving such hazardous materials are therefore likely to be extremely serious, and as many ports are close to densely populated areas, the risks are greatly increased (Chen et al., 2020). For example, the major explosion in the port of Beirut in August 2020 killed more than 100 people and injured over 4,000. This illustrates the urgency of improving the safety risk controls for hazardous materials in ports. Automated unmanned trucks are important components in the horizontal transportation retrofitting of ports. However, trucks in ports must comply with route, time, and speed regulations when transporting hazardous materials, and drivers are strictly prohibited from overtaking, speeding, tailgating, making sharp turns, and sudden braking. They must also keep a safe distance from other vehicles. Such operational tasks are extremely difficult for unmanned yard trucks (YTs), and thus we assume that hazardous material must be transported by manned trucks, while non-hazardous material can be transported by manned or unmanned trucks.

In this study, we propose an optimization model for the retrofitting and deployment of YTs that considers the transportation of hazardous material in green ports. In this two-stage stochastic programming model, the first stage determines the reasonable number of YTs to be purchased, retrofitted, and chartered and the second stage determines the number of workloads and those delayed in each time-step. We also propose a plan for the retrofitting of YTs from diesel to electricity or liquefied natural gas (LNG). Manned or unmanned YTs are applied

to different types of operation tasks depending on whether hazardous or non-hazardous materials are to be handled. We develop an enhanced Benders decomposition using a Lagrangian relaxation algorithm to solve the problem of YT retrofitting and deployment, and we find that an optimal solution can be obtained within a reasonable time. We focus on a port in Shanghai and conduct a numerical experiment, aiming to provide support for decisions regarding the sustainable development and operation of green ports.

The remainder of this paper is organized as follows. We present a review of the literature in Section 2. Section 3 describes the problem in detail and our stochastic programming mathematical model for the retrofitting and deployment of YTs. We develop the LR-BD algorithm in Section 4. Section 5 presents our extensive numerical experiments. The conclusions are provided in Section 6.

2. Literature review

Building green ports represents a major breakthrough in the shipping industry in terms of energy saving, emission reduction, and intelligent technology (Chen et al., 2019). The automation and environmental of transportation equipment have become central goals in recent port developments. However, although automation helps to reduce human error, it also incurs high costs (Carlo et al., 2014). YTs are essential because they transport containers between the terminal and the yard. Abdelmagid et al. (2014) and Carlo et al. (2014) have provided comprehensive overviews of YTs, and in this section, we present our own review of the recent literature, focusing on three streams.

The first stream is about the analytical studies for improving the operational efficiency of YTs. Zhang et al. (2019) proposed a truck reservation optimization model based on the non-stationary queuing theory aimed at reducing the waiting times of internal and external trucks in the yard and thus alleviating YT congestion. Their model can effectively improve calculation accuracy. Ramirez-Nafarrate et al. (2017) constructed a discrete-event simulation model by analyzing the potential configurations of a truck appointment system and evaluating its impact on reducing container rehandles and truck turnaround times. Zhang et al. (2019) established a bilevel programming model to determine optimal toll rates and thus alleviate truck congestion in container terminals. They designed a memetic heuristic algorithm to solve the model. Huang and Zheng (2016) proposed an improved ant colony optimization for the path planning of autonomous container trucks within the complex construction environments of container ports based on a rolling window. Islam (2018) developed a model simulating shared trucks in ports and found that they can effectively reduce truck emissions and improve the port's transportation capacity. Wang et al. (2014) proposed a strategy of owning and chartering trucks after combining internal truck

scheduling and storage allocation problems in the container terminal, and they applied a two-level heuristic algorithm to solve the model. He et al. (2013) proposed an internal truck assignment model aimed at minimizing the overflow of workloads and the costs of transferring. They explored the optimal decision-making for sharing internal trucks between multiple adjacent container terminals.

The second stream is the optimization deployment decisions with the objective of reducing YT pollution emissions. Heilig et al. (2017) solved the multi-objective inter-terminal truck routing problem by considering truck emissions and proposed a multi-objective archived simulated annealing algorithm and visualization technique. The aims of digitalization and optimization were integrated by embedding the algorithm into a cloud-based decision support system. Lee et al. (2019) proposed that emission control areas and affected zones should be established in Incheon Port. They suggested reducing gate congestion, limiting emissions, and minimizing the negative impact on local communities by developing an integrated information and truck appointment system. Schulte et al. (2017) analyzed a truck appointment system that had collaboration requirements and developed an optimization model based on the multiple traveling salesman problem with time windows to reduce emissions and costs. Clott and Hartman (2013) argued that limiting truck emissions through the Port of Los Angeles Clean Truck Programme would be extremely significant for the port and the shipping industry as a whole, and they applied game theoretical models to predict the potential effects of such truck conversion policies. Hartman and Clott (2012) constructed an economic model to minimize the cost of truck emission controls and collateral production changes so that throughput targets could be achieved in addition to emission constraints. Rowangould et al. (2018) identified that air pollution emissions from the activities of port trucks can threaten the health of nearby communities. They proposed that low-emission trucks should be used in ports to reduce the risks. Saharidis and Konstantzos (2018) reviewed 10 commonly used and highly cited emission calculation models and evaluated their potential for estimating GHG emissions from YT operations.

The third stream concerns green technology transformation and upgrading, including YT retrofit, energy substitution, and intelligent automation. Diesel-to-electricity retrofitting involves an efficient technology that saves energy and reduces emissions, but it involves problems such as the huge initial investment required and high electricity prices. For shipping companies, LNG, low-sulfur fuels, and other alternative sources of energy have become important for meeting emission reduction requirements (Lu & Huang, 2021). Seddiek (2020) demonstrated the techno-economic feasibility of using fuel cells and offshore wind turbines in a green energy strategy. Bailey and Solomon (2004) proposed that positive measures such as restrictions on truck idling rates and the utilization of low-sulfur diesel or alternative fuels can alleviate the health risks brought by port environmental

pollution. Zhong et al. (2019) established a nonlinear optimization model for carbon emission estimation and reduction and suggested that policy makers should encourage the use of LNG trucks and optimize the number and layouts of gas stations. Long operation times, high labor demand, and the risks brought by fatigued drivers have become major bottlenecks in traditional container terminals. The use of automated YTs for container transportation can address these problems through reducing labor costs, improving container throughput efficiency, ensuring continuous 24-hour operation, and increasing reliability (Zhang et al., 2006). Automated guided vehicles (AGVs), alternative equipment of YTs, are used to transport goods from the quayside to the yard and are commonly used in smart ports. Ji et al. (2020) and Xin et al. (2015) constructed an integrated scheduling bi-level programming model based on the conflict resolution strategy to address the conflict and congestion problems of AGVs and designed two bi-level optimization algorithms to solve the proposed models.

The consideration and application of clean energy is essential in the construction of green ports. The current research into YTs is mainly aimed at reducing waiting times, pollution, emissions, and congestion through the development of optimization models. Retrofitting or energy substitution in YTs has been considered, but carbon emissions quotas have not been integrated into the models. Sharing YTs between terminals represents a new trend in green port development. Research into automated terminals has generally focused on AGVs rather than unmanned trucks. Engineering construction such as laying magnetic nails and replacing fixtures is required for AGVs to be integrated into traditional ports and will consequently lead to major losses from shutdowns and high construction costs. An AGV is also much more expensive than an unmanned YT, and thus unmanned YTs are more suitable for retrofitting traditional ports. Safety is of the utmost importance when transporting hazardous material, but a fully automated port cannot easily handle the potential accidents from the transportation of hazardous cargo. Thus, a semi-automatic port that includes manned and unmanned YTs is often a better choice for such cargo.

Based on the above background analysis and literature review, we present an optimization model and algorithm for retrofitting and deploying YTs in the transportation of hazardous material in green ports. We propose retrofitting schemes for assigning various type of trucks, such as diesel-to-electricity YTs, diesel-to-LNG YTs, and manned or unmanned YTs, to different operational tasks in traditional yards. The LR-BD algorithm is designed to solve the model, and we compare and analyze its accuracy and efficiency.

3. Model formulation

3.1. Problem description

The appropriate type of container transportation equipment is an important strategic decision in the designing of green ports. The planning of YT retrofit and deployment can inform the strategic decisions that port operators must make in the development of green ports. The port operators must make two interrelated decisions to minimize the total operation costs and reduce pollution: the timing and planning of the YT retrofit and deployment. Most port operators plan their strategies on a monthly basis (one time-step). The YTs required and the total container handling workload do not typically change much within one time-step. Port operators must therefore reasonably allocate types and quantities of YTs according to the loading and unloading of containers, thus speeding up the container processing time (Steenken et al., 2004; Vis & de Koster, 2003).

The high levels of carbon dioxide (CO2) generated during the transportation operations of ports are a major cause of the greenhouse effect, and excessive CO2 emissions have a catastrophic impact on the global climate. Types of energy conversion such as diesel to electricity, diesel to gas, and others can help enterprises gain control over their carbon emissions, slow the global greenhouse effect, and provide economic benefits. Governments currently allocate a carbon emission quota to enterprises to encourage the development of green ports, and thus they do not have to pay if they remain within the standard. However, they must treat the excess emissions to ensure they are pollution-free.

Traditional manned diesel and electric YTs are the preferred tools for horizontal container transportation. As innovative technologies such as artificial intelligence, the internet of vehicles, cloud computing, green energy, and green materials evolve, unmanned electric and LNG YTs can be gradually introduced into a yard by configuring remote monitoring devices and on-board sensors. As Fig. 1 shows, traditional manned diesel YTs can be retrofitted into any other types of YTs, while traditional manned electric YTs can only be retrofitted into unmanned electric YTs. Unmanned electric and LNG YTs cannot be retrofitted.

YT operations may suffer from problems such as overweight containers or flammable, explosive, and highly toxic materials in the containers. Thus, ensuring the safety of YTs when handling overweight or hazardous materials is our focus, which can only be completed by traditional manned diesel or electric YTs. Drivers must abide by the safety management regulations for hazardous materials at ports, and the drivers' qualifications and YT standards are strictly controlled. In this study, other operations are defined as the transportation of non-hazardous materials, which can be completed by any type of YT.

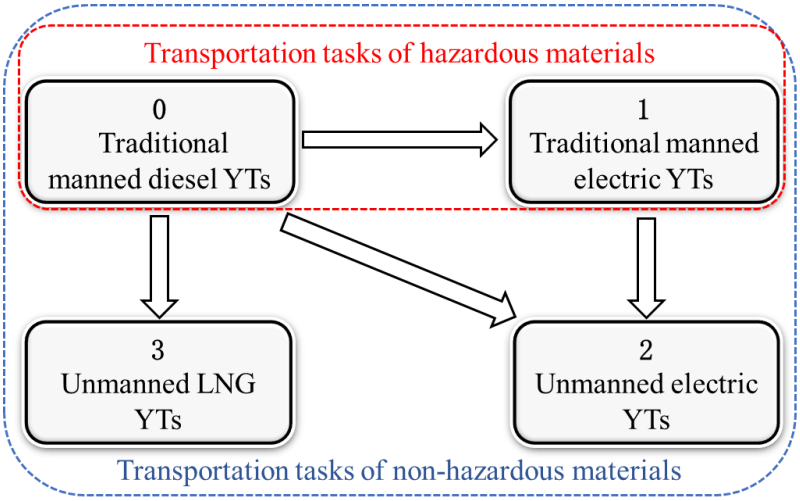

Figure 1: Conversion between different types of YTs and the corresponding transportation tasks

The imbalance between the peaks and troughs in terms of port activity is a challenge in port operations. To ensure the efficiency of terminals, it is necessary to integrate resources between multiple terminals and to implement the sharing of YTs. During the trough periods, idle YTs in the terminal can be chartered out for profit, and during peak periods, extra YTs can be chartered from adjacent terminals to ensure that operations are efficient at lower costs.

3.2. Assumptions

we make the following assumptions:

Assumption 1: At least one type of YT can be utilized for each type of task at any time-step.

Assumption 2: The carbon emission quota allocated by the government to the container terminal is limited and will remain unchanged during the planning period.

Assumption 3: The number of shared YTs between terminals is limited.

3.3. Notation

3.3.1. Indices and sets

K set of YTs types, indexed by k, $k \in K = \{0,1,2,3\}$, 0 means traditional manned diesel YTs, 1 means traditional manned electric YTs, 2 means unmanned electric YTs, 3 means unmanned LNG YTs.

T set of time-steps, indexed by t, $t \in \{1,2,\dots,T\}$.

L set of task types, indexed by l, $l \in L = \{0,1\}$, 0 means transportation tasks of non-hazardous materials, it can be operated by any YTs. 1 means transportation tasks of hazardous materials which require experienced manned drivers to operate the YTs.

S set of scenarios, indexed by s, $s \in \{1,2,\dots,S\}$.

3.3.2. Parameters

The first stage:

n_k the number of k-type YTs in traditional yards, $k \in \{0,1\}$.

$z_{k,t}$ maximum number of k-type shared YTs that can be chartered from other terminals during time-step t.

$e_{k,l}$ per unit carbon emissions generated by k-type YTs when operating l-type tasks.

c^o pollution-free treatment cost of per ton carbon emissions.

$c^v_{k,k'}$ the cost of retrofitting from k-type YTs into k'-type YTs.

c^b_k the cost of purchasing a new k-type YT.

c^{zr}_k charter in cost of a k-type shared YT.

c^{zc}_k charter out revenue a k-type shared YT.

$w_{k,l}$ If the k-type YTs can be operated in the l-type tasks, $w_{k,l} = 1,\ w_{k,l} = 0$ otherwise.

E_t carbon emission quota allocated by government in time-step t.

Q maximum number of YTs that can be accommodated in the yard.

F low carbon development funds available for container terminals.

M a sufficiently large positive number.

The second stage:

$c_{k,l}$ unit operating cost of l-type tasks operated by k-type YTs.

c^p_t penalty cost of per unit delayed workload in time-step t.

$h_{t,l,s}$ increased workloads of l-type tasks during time-step t under scenario s.

$q_{k,l}$ maximum operation capacity of l-type tasks operated by k-type YTs.

ρ_s possibility of occurrence of scenario s.

3.3.3. Decision variables

The first stage:

$\alpha_{k,t,l}$ number of k-type YTs operated in l-type tasks during time-step t.

$\mu_{k,t}$ number of k-type YTs during time-step t.

$\beta_{k,k',t}$ number of k-type YTs retrofitted to k'-type YTs during time-step t.

$\gamma_{k,t}$ number of k-type YTs purchased during time-step t.

$\eta_{k,t}$ number of k-type YTs chartered in during time-step t.

$\varepsilon_{k,t}$ number of k-type YTs chartered out during time-step t.

$\omega_{k,t,l}$ If the k-type YTs can be operated in l-type tasks during time-step t $\omega_{k,t,l} = 1$,. $\omega_{k,t,l} = 0$ otherwise.

The second stage:

$\theta_{k,t,l,s}$ the number of workloads of l-type tasks operated by k-type YTs during time-step t under scenario s.

$\lambda_{t,l,s}$ the number of delayed workloads of l-type tasks that cannot be operated during time-step t under scenario s

3.4. Mathematical model

$$Min \ \sum_{k\in K}\sum_{t\in T}(c_k^b\cdot\gamma_{k,t}+c_k^{zr}\cdot\eta_{k,t}-c_k^{zc}\cdot\varepsilon_{k,t}+\sum_{k'\in K:k\neq k'}c_{k,k'}^{v}\cdot\beta_{k,k',t})+c^o\cdot\sum_{t\in T}\Big[\sum_{k\in K}\sum_{l\in L}\big(e_{k,l}\cdot\alpha_{k,t,l}\big)-E_t\Big]+\sum_{s\in S}\rho_s\cdot\mathcal{G}(\boldsymbol{\beta},\boldsymbol{h}) \quad (1)$$

$s.t.$

$$\mu_{k,0}=n_k, \qquad \forall k\in\{0,1\} \quad (2)$$

$$\mu_{k,0}=0, \qquad \forall k\in\{2,3\} \quad (3)$$

$$\mu_{k,t}=\mu_{k,t-1}+\gamma_{k,t}+\eta_{k,t}+\sum_{k'\in K:k'\neq k}\beta_{k',k,t}-\varepsilon_{k,t}-\sum_{k'\in K:k'\neq k}\beta_{k,k',t}, \qquad \forall k\in K,\forall t\in T:t\neq 0 \quad (4)$$

$$\sum_{k'\in K:k'\neq k}\beta_{k,k',t}\leq\mu_{k,t-1}, \qquad \forall k\in K,\forall t\in T:t\neq 0 \quad (5)$$

$$\eta_{k,t}\leq z_{k,t}, \qquad \forall k\in K,\forall t\in T \quad (6)$$

$$\eta_{k,t}\leq\Big(\left\lceil\frac{\sum_{l\in L}(h_{t,l,s}+\lambda_{t-1,l,s})}{q_{k,l}}\right\rceil-\mu_{k,t-1}\Big)^+, \qquad \forall k\in K,\forall t\in T:t\neq 0,\forall s\in S \quad (7)$$

$$\varepsilon_{k,t}\leq\big(\mu_{k,t-1}-M\cdot\lambda_{t-1,l,s}\cdot w_{k,l}\big)^+, \qquad \forall k\in K,\forall t\in T:t\neq 0,\forall l\in L,\forall s\in S \quad (8)$$

$$c^o\cdot\sum_{t\in T}\Big[\sum_{k\in K}\sum_{l\in L}\big(e_{k,l}\cdot\alpha_{k,t,l}\big)-E_t\Big]\leq F, \quad (9)$$

$$\alpha_{k,t,l}\leq M\cdot w_{k,l}, \qquad \forall k\in K,\forall t\in T,\forall l\in L \quad (10)$$

$$\alpha_{k,t,l}\leq\mu_{k,t}\cdot\omega_{k,t,l}, \qquad \forall k\in K,\forall t\in T,\forall l\in L \quad (11)$$

$$\sum_{k\in K}\omega_{k,t,l}\geq 1, \qquad \forall t\in T,\forall l\in L \quad (12)$$

$$\omega_{k,t,l}\leq w_{k,l}, \qquad \forall k\in K,\forall t\in T,\forall l\in L \quad (13)$$

$$\sum_{k\in K}\mu_{k,t}\leq Q, \qquad \forall t\in T \quad (14)$$

$$\omega_{k,t,l}\in\{0,1\}, \qquad \forall k\in K,\forall t\in T,\forall l\in L \quad (15)$$

$$\alpha_{k,t,l},\mu_{k,t},\beta_{k,k',t},\gamma_{k,t},\eta_{k,t},\varepsilon_{k,t}\in\mathbb{N}^+, \qquad \forall k,k'\in K:k\neq k',\forall t\in T,\forall l\in L \quad (16)$$

where $\mathcal{G}(\boldsymbol{\beta},\boldsymbol{h})$ in the objective function (1) is the optimal value of the following model:

$$Min \ \sum_{k\in K}\sum_{t\in T}\sum_{l\in L}(c_{k,l}\cdot\theta_{k,t,l,s})+\sum_{t\in T}\sum_{l\in L}(c_t^p\cdot\lambda_{t,l,s}) \tag{17}$$

$$\theta_{k,t,l,s}\le\alpha_{k,t,l}\cdot q_{k,l}, \qquad \forall k\in K,\forall t\in T,\forall l\in L,\forall s\in S \tag{18}$$

$$\sum_{k\in K}\theta_{k,t,l,s}\le h_{t,l,s}+\lambda_{t-1,l,s}, \qquad \forall t\in T: t\neq 0,\forall l\in L,\forall s\in S \tag{19}$$

$$\lambda_{0,l,s}=h_{0,l,s}-\sum_{k\in K}\theta_{k,0,l,s}, \qquad \forall l\in L,\forall s\in S \tag{20}$$

$$\lambda_{t,l,s}=\lambda_{t-1,l,s}+h_{t,l,s}-\sum_{k\in K}\theta_{k,t,l,s}, \qquad \forall l\in L,\forall t\in T: t\neq 0,\forall s\in S \tag{21}$$

$$\theta_{k,t,l,s},\lambda_{t,l,s}\ge 0, \qquad \forall k\in K,\forall t\in T,\forall l\in L,\forall s\in S \tag{22}$$

The objective function (1) represent the total cost of minimizing the YTs retrofit and deployment for green ports, including purchase costs, charter in costs, charter out revenues, retrofit costs, carbon emissions pollution-free treatment costs, operation costs, and delay penalty costs. Constraint (2) indicates that the number of traditional diesel and electric YTs in the initial time-step is determined by the number of the YTs possessed in the traditional yard. Constraint (3) ensures that there are no unmanned electric and LNG YTs in the initial time-step. Constraint (4) means that the number of k-type YTs during the time-step t is affected by the number of YTs held, purchased, retrofitted, chartered during time-step $t-1$. Constraint (5) guarantees that the number of k-type YTs, those can be retrofitted during time-step t, should be no more than the number of k-type YTs during time-step $t-1$. Constraint (6) enforces that the k-type shared YTs chartered in time-step t should be less than the maximum number of shared YTs that can be chartered from other terminals. Constraint (7) indicates that the number of k-type YTs that can be chartered during time-step t is affected by the number of workloads to be completed. The number of chartered YTs is determined by the number of those held in time-step $t-1$ and required in the time-step t. $\left\lceil\frac{\sum_{l\in L}(h_{t,l,s}+\lambda_{t-1,l,s})}{q_k}\right\rceil$ calculates the minimum number of YTs required for the operation of the new workloads in time-step t and the delayed workloads in time-step $t-1$ (take an integer upward). $\left(\left\lceil\frac{\sum_{l\in L}(h_{t,l,s}+\lambda_{t-1,l,s})}{q_k}\right\rceil-\mu_{k,t-1}\right)^+$ represents the minimum number of YTs required for the operation of the workloads in time-step t minus the number of YTs held in time-step $t-1$. If greater than 0, this value is the minimum number of YTs that needs to be chartered from other terminals. If less than or equal to 0, the number of YTs held in time-step t is sufficient to operate the pending workloads, and it is not necessary to charter YTs from other terminals. Constraint (8) limits the number of k-type YTs can be chartered out in time period t, which should be no more than that in time-step $t-1$. When the number of delayed workloads in the last time-step $\lambda_{t-1,l,s}>0$, judge whether the k-type YTs will be judged whether they are competent to l-type tasks, if $w_{k,l}=1$, the YTs are not allowed to charter out, $w_{k,l}=0$ otherwise. When the number of delayed workloads in the last time-step $\lambda_{t-1,l,s}=0$, the YTs are allowed to charter

out. Constraint (9) addresses that the pollution-free treatment costs of carbon emissions are limited by the investment of low-carbon development funds. Constraint (10) states that the number of k-type YTs used in the operation of l-type tasks in time-step t is affected by whether the type of tasks can be operated. Constraint (11) represents the number of YTs used in the operation of l-type tasks is limited by the number of YTs held during the time-step t and whether the YTs can be used in the operation of l-type tasks. Constraint (12) guarantees that at least one type of YTs can be utilized in the operation of l-type tasks during the time-step t. Constraint (13) restricts the operations of l-type tasks by k-type YTs at any time-step. Constraint (14) limits the capacity of the YTs in the yard. Constraint (15) defines $\omega_{k,t,l}$ as binary variable. Constraint (16) defines decision variables $\alpha_{k,t,l}, \mu_{k,t}, \beta_{k,k',t}, \gamma_{k,t}, \eta_{k,t}, \varepsilon_{k,t}$ as positive integers. Constraint (18) limits the maximum operating capacity of the YTs. Constraint (19) enforces that the workloads of l -type tasks operated by YTs during time-step t under any scenario cannot exceed the sum of the increased workloads in time-step t and the delayed workloads in time-step $t-1$. Constraint (20) states the delayed workloads in the initial time step. Constraint (21) provides the delayed workloads in time-step t. Constraint (22) defines the decision variables $\theta_{k,t,l,s}, \lambda_{t,l,s}$ as positive real numbers.

Constraint (7) can be expressed as $\eta_{k,t} \leq max\left\{\left\lceil\frac{\sum_{l\in L}(h_{t,l,s}+\lambda_{t-1,l,s})}{q_k}\right\rceil - \mu_{k,t-1}, 0\right\}$, linearized by defining the binary variables ρ_1, ρ_2 to, added variables and constraints are expressed as follows.

Added variables

ρ_1, ρ_2, the binary variable, auxiliary variable to linearize constraint (7).

Added Constraints

$$\eta_{k,t} \leq \left\lceil\frac{\sum_{l\in L}(h_{t,l,s}+\lambda_{t-1,l,s})}{q_k}\right\rceil - \mu_{k,t-1} + M(1-\rho_1), \qquad \forall k \in K, \forall t \in T: t \neq 0, \forall s \in S \tag{23}$$

$$\eta_{k,t} \leq M(1-\rho_2), \qquad \forall k \in K, \forall t \in T \tag{24}$$

$$\rho_1 + \rho_2 \geq 1, \tag{25}$$

$$\rho_1, \rho_2 \in \{0,1\}, \tag{26}$$

Similar to constraint (7), constraint (8) can be expressed as $\varepsilon_{k,t} \leq max\{\mu_{k,t-1} - M \cdot \lambda_{t-1,l,s} \cdot w_{k,l}, 0\}$, linearized by defining the binary variables ρ_3, ρ_4 to, added variables and constraints are expressed as follows.

Added variables

ρ_3, ρ_4, the binary variable, auxiliary variable to linearize constraint (8).

Added constraints

$$\varepsilon_{k,t} \leq \mu_{k,t-1} - M \cdot \lambda_{t-1,l,s} \cdot w_{k,l} + M(1-\rho_3), \qquad \forall k \in K, \forall t \in T: t \neq 0, \forall l \in L, \forall s \in S \tag{27}$$

$$\varepsilon_{k,t} \le M(1-\rho_4), \qquad \forall k \in K, \forall t \in T \tag{28}$$

$$\rho_3 + \rho_4 \ge 1, \tag{29}$$

$$\rho_3, \rho_4 \in \{0,1\}, \tag{30}$$

Constraint (11) $\alpha_{k,t,l} \le \mu_{k,t} \cdot \omega_{k,t,l}$ involves the multiplication of two decision variables into a nonlinear constraint, by defining the binary variable $\pi_{k,t,l,i}$ to linearize constraint (11), added set, variable and constraints are expressed as follows.

Added set

I set of the number of YTs, indexed by i.

Added variable

$\pi_{k,t,l,i}$ the binary variable, the number of k-type YTs can be operated for l-type tasks during time-step t is i, $\pi_{k,t,l,i} = 1$; $\pi_{k,t,l,i} = 0$ otherwise.

Added constraints

$$\alpha_{k,t,l} \le \sum_{i \in I}(\pi_{k,t,l,i} \cdot i) \qquad \forall k \in K, \forall t \in T, \forall l \in L \tag{31}$$

$$\pi_{k,t,l,i} \le \omega_{k,t,l}, \qquad \forall k \in K, \forall t \in T, \forall l \in L, \forall i \in I \tag{32}$$

$$\sum_{i \in I} \pi_{k,t,l,i} = \omega_{k,t,l}, \qquad \forall k \in K, \forall t \in T, \forall l \in L \tag{33}$$

$$\sum_{i \in I}(\pi_{k,t,l,i} \cdot i) \le \mu_{k,t}, \qquad \forall k \in K, \forall t \in T, \forall l \in L \tag{34}$$

$$\sum_{i \in I}(\pi_{k,t,l,i} \cdot i) \ge \mu_{k,t} + M\left(\omega_{k,t,l} - 1\right), \qquad \forall k \in K, \forall t \in T, \forall l \in L \tag{35}$$

4. An enhanced Benders decomposition using Lagrangian relaxation approach

4.1. Classical Benders decomposition

The Benders decomposition algorithm was first proposed by Jacques F. Benders in 1962 to solve large-scale mixed integer programming problems (Benders, 1962). When the integer variables are fixed, the continuous linear programming problem can be solved by dual theory (Rahmaniani et al., 2017). BD algorithm has been widely used in two-stage stochastic linear programming problems (Caroe & Tind, 1998; Clay & Grossmann, 1997; Noyan, 2012; Noyan et al., 2016).

According to the principle of the BD algorithm and the characteristics of the model proposed in this paper, the model can be divided into two stages. In the first stage, the decision variables $\alpha_{k,t,l}, \beta_{k,k',t}, \gamma_{k,t}, \eta_{k,t}, \varepsilon_{k,t}, \mu_{k,t}, \omega_{k,t,l}$ related to the number of YTs are determined, these variables are integer variables and 0-1 variables—complex variables. When the complex variables are fixed, the remaining optimization problems will be easier to be solved.

This part is called the master problem (MP). In the second stage, the decision variables $\theta_{k,t,l,s}, \lambda_{t,l,s}$ related to the workloads and delayed workloads are determined. These two variables are continuous variables, and this part is called the subproblem (SP).

We let $\bar{\alpha}_{k,t,l}$ denotes the vector of fixed $\alpha_{k,t,l}$ variables. The expected operating and penalty cost of the second-stage decisions, denoted by $v(\bar{\alpha}_{k,t,l})$, can be calculated as $v(\bar{\alpha}_{k,t,l}) = \sum_{x \in X} \rho_s v_s(\bar{\alpha}_{k,t,l})$, where $v_s(\bar{\alpha}_{k,t,l})$ is the expected operating and penalty cost under scenario s, which can be obtained by solving the following primal subproblem:

[SP] $$v_s(\bar{\alpha}_{k,t,l}) = Min \quad \sum_{k \in K} \sum_{t \in T} \sum_{l \in L} (c_{k,l} \cdot \theta_{k,t,l,s}) + \sum_{t \in T} \sum_{l \in L} (c_t^p \cdot \lambda_{t,l,s}) \tag{36}$$

$s.t.$

$$\theta_{k,t,l,s} \leq \hat{\alpha}_{k,t,l} \cdot q_{k,l}, \qquad \forall k \in K, \forall t \in T, \forall l \in L, \forall s \in S \tag{37}$$

$$\sum_{k \in K} \theta_{k,t,l,s} \leq h_{t,l,s} + \lambda_{t-1,l,s}, \qquad \forall t \in T: t \neq 0, \forall l \in L, \forall s \in S \tag{38}$$

$$\lambda_{0,l,s} = h_{0,l,s} - \sum_{k \in K} \theta_{k,0,l,s}, \qquad \forall l \in L, \forall s \in S \tag{39}$$

$$\lambda_{t,l,s} = \lambda_{t-1,l,s} + h_{t,l,s} - \sum_{k \in K} \theta_{k,t,l,s}, \qquad \forall l \in L, \forall t \in T: t \neq 0, \forall s \in S \tag{40}$$

$$\theta_{k,t,l,s}, \lambda_{t,l,s} \geq 0, \qquad \forall k \in K, \forall t \in T, \forall l \in L, \forall s \in S \tag{41}$$

Due to the presence of the variable $\lambda_{t,l,s}$, the SP is always feasible because the workloads can be delayed. Furthermore, since the cost parameters $c_{k,l}$ and c_t^p are finite and due to constraints (38) – (40), any feasible solution of the SP must be bounded. Hence, the dual of SP is feasible and bounded.

Let $\varphi^1 = (\varphi^1_{k,t,l,s} \leq 0 | \forall k \in K, \forall t \in T, \forall l \in L, \forall s \in S)$, $\varphi^2 = (\varphi^2_{t,l,s} \leq 0 | \forall t \in T: t \neq 0, \forall l \in L, \forall s \in S)$, $\varphi^3 = (\varphi^3_{t,l,s} | \forall t \in T: t = 0, \forall l \in L, \forall s \in S)$, $\varphi^4 = (\varphi^4_{t,l,s} | \forall t \in T: t \neq 0, \forall l \in L, \forall s \in S)$ denote the vectors of the dual variables associated with constraints (37) – (41), respectively. The dual of primal subproblem under each scenario s, called the dual subproblem (DSP), can be formulated as follows:

[DSP] $$v_s(\bar{\alpha}_{k,t,l}) = Max \quad \sum_{k \in K} \sum_{t \in T} \sum_{l \in L} (\varphi^1_{k,t,l,s} \cdot \bar{\alpha}_{k,t,l} \cdot q_{k,l}) + \sum_{t \in T: t \neq 0} \sum_{l \in L} (\varphi^2_{t,l,s} \cdot h_{t,l,s}) + \sum_{t \in T: t=0} \sum_{l \in L} (\varphi^3_{t,l,s} \cdot h_{t,l,s}) + \sum_{t \in T: t \neq 0} \sum_{l \in L} (\varphi^4_{t,l,s} \cdot h_{t,l,s}) \tag{42}$$

$s.t.$

$$\varphi^1_{k,0,l,s} + \varphi^3_{0,l,s} \leq c_{k,l}, \qquad \forall k \in K, \forall l \in L, \forall s \in S \tag{43}$$

$$\varphi^1_{k,t,l,s} + \varphi^2_{t,l,s} + \varphi^4_{t,l,s} \leq c_{k,l}, \qquad \forall k \in K, \forall t \in T: t \neq 0, \forall l \in L, \forall s \in S \tag{44}$$

$$-\varphi^2_{t+1,l,s} + \varphi^3_{t,l,s} - \varphi^4_{t+1,l,s} \leq c_t^p, \qquad \forall t \in T: t = 0, \forall l \in L, \forall s \in S \tag{45}$$

$$-\varphi^2_{t+1,l,s} + \varphi^4_{t,l,s} - \varphi^4_{t+1,l,s} \leq c_t^p, \qquad \forall t \in T: t \neq 0, \forall l \in L, \forall s \in S \tag{46}$$

$$\varphi^1_{k,t,l,s}, \varphi^2_{t,l,s} \le 0, \qquad \forall k \in K, \forall t \in T, \forall l \in L, \forall s \in S \tag{47}$$

$$\varphi^3_{t,l,s}, \varphi^4_{t,l,s} \sim free, \qquad \forall t \in T, \forall l \in L, \forall s \in S \tag{48}$$

According to the solution of the DSP, we introduce an extra variable Φ representing the expected operating cost and penalty cost. we add optimality cuts into the master problem (MP) to reduce the search region. The MP that provides a valid lower bound for the initial problem can be reformulated as follows:

$$\textbf{[MP]} \quad Min \quad \sum_{k\in K}\sum_{t\in T}(c^b_k \cdot \gamma_{k,t} + c^{zr}_k \cdot \eta_{k,t} - c^{zc}_k \cdot \varepsilon_{k,t} + \sum_{k'\in K:k\neq k'} c^v_{k,k'} \cdot \beta_{k,k',t}) + c^o \cdot \sum_{t\in T}\left[\sum_{k\in K}\sum_{l\in L}\left(e_{k,l} \cdot \alpha_{k,t,l}\right) - E_t\right] + \Phi \tag{49}$$

$s.t.$ constraints (2) – (16).

$$\sum_{s\in S}\rho_s \left[\sum_{k\in K}\sum_{t\in T}\sum_{l\in L}(\bar{\varphi}^1_{k,t,l,s} \cdot \alpha_{k,t,l} \cdot q_{k,l}) + \sum_{t\in T:t\neq 0}\sum_{l\in L}(\bar{\varphi}^2_{t,l,s} \cdot h_{t,l,s}) + \sum_{t\in T:t=0}\sum_{l\in L}(\bar{\varphi}^3_{t,l,s} \cdot h_{t,l,s}) + \sum_{t\in T:t\neq 0}\sum_{l\in L}(\bar{\varphi}^4_{t,l,s} \cdot h_{t,l,s})\right] \le \Phi, \qquad \forall(\varphi^1, \varphi^2, \varphi^3, \varphi^4) \in \Delta^s \tag{50}$$

Constraints (50) is the optimality cut that is valid with any feasible solutions of MP and of DSP. Where Δ^s denotes the set of extreme points of the polyhedron defined by the constraints of the SP.

4.2. Pareto optimal cut

To improve the calculation performance of the classical BD algorithm, it is necessary to constantly seek for better cutting-plane generation schemes (Watson & Rogers, 2007). Magnanti and Wong (1981) proposed the use of Pareto optimal cuts to generate high-quality feasible solutions and to reduce solution time. To obtain the Pareto optimal cut, a new DSP based on a set of core point ($\alpha^0_{k,t,l}$) is dissolved. $v_s(\bar{\alpha}_{k,t,l})$ is the optimal value of the objective function of the primal DSP (Adulyasak et al., 2015; K. Wang & Jacquillat, 2020). A Pareto optimal cut can be obtained by solving the following subproblem:

$$Max \quad \sum_{k\in K}\sum_{t\in T}\sum_{l\in L}\left(\varphi^1_{k,t,l,s} \cdot \alpha^0_{k,t,l} \cdot q_{k,l}\right) + \sum_{t\in T:t\neq 0}\sum_{l\in L}\left(\varphi^2_{t,l,s} \cdot h_{t,l,s}\right) + \sum_{t\in T:t=0}\sum_{l\in L}(\varphi^3_{t,l,s} \cdot h_{t,l,s}) + \sum_{t\in T:t\neq 0}\sum_{l\in L}(\varphi^4_{t,l,s} \cdot h_{t,l,s}) \tag{51}$$

$s.t.$ constraints (43) – (48).

$$\sum_{k\in K}\sum_{t\in T}\sum_{l\in L}\left(\varphi^1_{k,t,l,s} \cdot \bar{\alpha}_{k,t,l} \cdot q_{k,l}\right) + \sum_{t\in T:t\neq 0}\sum_{l\in L}\left(\varphi^2_{t,l,s} \cdot h_{t,l,s}\right) + \sum_{t\in T:t=0}\sum_{l\in L}(\varphi^3_{t,l,s} \cdot h_{t,l,s}) + \sum_{t\in T:t\neq 0}\sum_{l\in L}(\varphi^4_{t,l,s} \cdot h_{t,l,s}) = v_s(\bar{\alpha}_{k,t,l}), \qquad \forall(\varphi^1, \varphi^2, \varphi^3, \varphi^4) \in \Delta^s \tag{52}$$

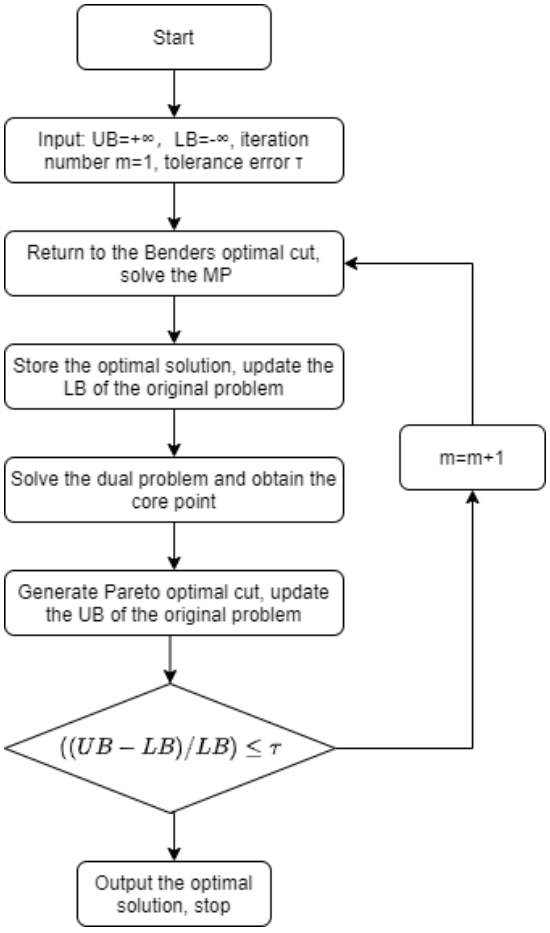

Figure 2: Flow chart of BD using Pareto optimal cut acceleration

4.3. Enhanced Benders decomposition using Lagrangian relaxation (LR-BD)

Lagrangian relaxation (LR) is an algorithm for solving the lower bound (LB) of constrained programming problem. It makes the problem easier to solve by absorbing the constraints, which make the problem difficult to solve, into the objective function (Zhen, 2017).

We relax complex constraints (5) by introducing Lagrangian multipliers $\sigma_{k,t}$ ($\forall k \in K, \forall t \in T: t \neq 0$), making the problem easier to solve. The Lagrangian relaxation problem $LR(\sigma)$ becomes as follows:

$$[\boldsymbol{LR(\sigma)}] \quad Min \quad \sum_{k\in K}\sum_{t\in T}(c_k^b \cdot \gamma_{k,t} + c_k^{zr} \cdot \eta_{k,t} - c_k^{zc} \cdot \varepsilon_{k,t} + \sum_{k'\in K:k\neq k'} c_{k,k'}^{v} \cdot \beta_{k,k',t}) + c^o \cdot$$

$$\sum_{t\in T}\left[\sum_{k\in K}\sum_{l\in L}\left(e_{k,l} \cdot \alpha_{k,t,l}\right) - E_t\right] + \sum_{s\in S}\rho_s\left[\sum_{k\in K}\sum_{t\in T}\sum_{l\in L}(c_{k,l} \cdot \theta_{k,t,l,s}) + \sum_{t\in T}\sum_{l\in L}\left(c_t^p \cdot \lambda_{t,l,s}\right)\right] +$$

$$\sum_{k\in K}\sum_{t\in T}\left(\sum_{k'\in K:k'\neq k}\beta_{k,k',t} - \mu_{k,t-1}\right) \tag{53}$$

$s.t.$ Constraints (2) – (4), and (6) – (22).

The objective function value of the LR problem is the LB of the original problem model. The Lagrangian dual problem is defined as follow:

$$[\boldsymbol{LD}] \quad \max \; LR(\sigma). \tag{54}$$

Find the extreme value of the objective function along the subgradient direction at one point.

Let $(\mu^m,\ \beta^m)$ be the optimal solution of $LR(\sigma)$ at iteration m $(m \geq 0)$. Denoting

$$\zeta_{k,t}^m = \sum_{k' \in K: k' \neq k} \beta_{k,k',t}^m - \mu_{k,t-1}^m, \qquad \forall k \in K, \forall t \in T: t \neq 0 \tag{55}$$

In the next iteration of $m+1$, the Lagrangian multiplier is updated to

$$\sigma_{k,t}^{m+1} = \max\{0,\ \sigma_{k,t}^m + \varpi^m \cdot \zeta_{k,t}^m\} \tag{56}$$

Where the step-size ϖ^m is expressed as

$$\varpi^m = \frac{\xi^m \cdot \left(UB - LR(\sigma_{k,t}^m)\right)}{\sum_{k \in K} \sum_{t \in T} \left(\zeta_{k,t}^m\right)^2} \tag{57}$$

In constraints (57), ξ^m is a parameter in the interval [0,2], which is called the step adjustment factor, and generally takes $\xi^0 = 2$. When the value of the objective function of $LR(\sigma)$ increases, ξ^m does not change. When the value of the objective function of $LR(\sigma)$ does not change in a given number of consecutive iterations, half of ξ^m is taken. UB is the minimum upper bound value corresponding to the feasible solution of the original problem. The initial UB can be estimated. Judge whether the current solution is a feasible solution in the iteration. If it is a feasible solution and the objective function value is less than the current UB, update UB. $LR\left(\sigma_{k,t}^m\right)$ is the LB of the original problem obtained in the mth iteration.

The iteration is terminated if any of the following conditions are met: (i) $UB = LR\left(\sigma_{k,t}^m\right)$, (ii) step adjustment factor $\xi^m < 0.0001$, or (iii) number of iterations $m > 100$.

Substitute the current optimal value of each decision variable obtained by the LR into the MP of the BD to solve the solution. The feasible upper bound (UB) and good cut obtained by LR-BD greatly reduces the number of iterations of BD, and improves the efficiency of the algorithm. The detailed steps for enhanced Benders decomposition using Lagrangian relaxation are provided in Appendix A.

5. Numerical experiments

To verify the effectiveness of the proposed algorithm, numerical experiments including performance analysis and sensitivity analysis are carried out in this paper. The quality and processing time of LR-BD, PSO-BD and CPLEX for small-scale problems are compared, and the advantages of LR-BD are compared with PSO-BD for large-scale problems. The Central Processing Unit (CPU) of the experimental platform used in this paper is Intel Xeon E5-2643 v4 3.4Ghz. The models are solved in CPLEX 12.6.1 and programmed in C# (Visual Studio 2015).

5.1. Experimental setting

Taking a port in Shanghai as an example, the monthly containers throughput was about 560,000 to 800,000 twenty-feet equivalent units (TEUs) (Tan et al., 2021). The cost of pollution-free treatment of CO_2 obeys uniform distribution U (0.21,0.42) RMB (Cheng, 2020). The carbon emissions $e_{k,l}$ of a YT is equal to the carbon emissions per TEU multiplied by the number of YT operation TEUs per time-step. Among them, the carbon emissions of diesel YT operation per TEU is 0.592kg, and the LNG YT is 0.435kg (Huang Cheng & Jie, 2019). Assuming that the delay penalty cost c_t^p per workload unit is 500 RMB, the maximum $z_{k,t}$ of k-type shared YTs that can be chartered from other terminals in per time-step obeys the discrete random number of uniform distribution U (5,8), and the rental cost c_k^{zr} of a YT obeys uniform distribution of U (50,80) thousand RMB, rental income obeys uniform distribution U (30,50) thousand RMB, free carbon emission quota E_t obeys uniform distribution U (1000,2000) RMB, and the maximum number of YTs that can be accommodated in the yard Q is 400. The retrofit cost of YT $c_{k,k'}^v$ is shown in Table 1. Other parameters of the experiment used in this paper are shown in Table 2.

Table 1: The retrofit cost of YT $c_{k,k'}^v$

The retrofit cost of YT (million RMB) (Anonymous, 2020)	Traditional electric YTs	Unmanned electric YTs	Unmanned LNG YTs
Traditional diesel YTs	11.85	20 (valuation)	U(7,9.5)
Traditional electric YTs	—	8	—

Table 2: Parameter definition

Parameter	Tasks type	Traditional diesel YTs	Traditional electric YTs	Unmanned electric YTs	Unmanned LNG YTs
$q_{k,l}$ (TEU)	General tasks	10800	21600	17280 (valuation)	11600
	Difficult tasks	6480 (valuation)	12960 (valuation)	—	—
$c_{k,l}$ (RMB) (Huang Cheng & Jie, 2019)	General tasks	7.213	1.185 (valuation)	1.185 (valuation)	5.122
	Difficult tasks	14.426	2.37	—	—
c_k^b (RMB) (Chen, 2016)	—	300600	350000 (valuation)	450000 (valuation)	366500

5.2. Computational results of the Benders decomposition based method

In this section, an enhanced Benders decomposition using particle swarm optimization (PSO-BD) is designed

(Appendix B). The results obtained by LR-BD and PSO-BD are presented. The computational performances of both approaches are compared and analyzed.

We design six experiments to test whether the algorithms can obtain satisfactory solutions in a reasonable time. The parameter settings of each experiment are shown in Table 3, in which ISG1 to ISG4 refer to small-scale experiments and ISG5 and ISG6 refer to large-scale experiments.

Table 3: Settings of experiments

Instance ID	T	n_0	Q	X
ISG1	6	20	200	100
ISG2	12	20	200	200
ISG3	18	20	200	300
ISG4	24	20	200	300
ISG5	30	25	300	400
ISG6	36	25	300	400

For the small-scale instances, we conduct a comparative analysis of CPLEX, LR-BD, and PSO-BD and present the results in Table 4. LR-BD can obtain the optimal solution within a significantly shorter solution time than CPLEX, and the number of iterations is drastically reduced. The gap between the LR-BD and CPLEX optimal solution is 0.00%. The quality of the solution obtained by the PSO-BD algorithm is poorer than that of LR-BD and is affected by randomness, and it thus easily falls into the local optimum.

For example, the optimal solution for the minimum total operating costs of the green port obtained by the CPLEX solver is 130,758,934 RMB for ID 1-6 in ISG2, and the running time is 563 seconds. The objective function value of the LR-BD algorithm that we propose is the same as the value of CPLEX, but the running time of LR-BD is significantly shorter, as it only needs 138 seconds. The heuristic algorithm PSO is used to optimize BD and improve its running speed. The objective function value obtained by PSO-BD is 131,969,732 RMB, the gap between it and the optimal solution is 0.93%, and the running time is 342 seconds.

CPLEX takes too long to solve the problem in the large-scale experimental scenarios, and thus LR-BD and PSO-BD are used to solve the model in this paper. For example, ID 2-1 in ISG5 indicates that the LR-BD algorithm only needs 1225 seconds to obtain the optimal solution, while PSO-BD takes 1924 seconds to produce an approximate solution, giving a gap of 4.81%. PSO-BD does not perform well in terms of convergence speed and solution quality compared to LR-BD. Thus, LR-BD solves the original model more quickly and effectively.

Table 4: Comparison among CPLEX, LR-BD, and PSO-BD in solving small-scale instances

Instance		**CPLEX**		**LR-BD**		**PSO-BD**		**Gap1**	**Gap2**
Scale	ID	OBJ	Time(s)	OBJ	Time(s)	OBJ	Time(s)		
(1)	(2)	(3)	(4)	(5)	(6)	(7)	(8)	((5)-(3))/(3)	((7)-(3))/(3)
	1-1	138286252	85	138286252	25	139045184	90	0.00%	0.55%
	1-2	116279255	63	116279255	23	117253808	88	0.00%	0.84%
ISG1	1-3	97850316	71	97856374	24	98659330	93	0.01%	0.83%
	1-4	124450220	68	124450220	23	125457559	92	0.00%	0.81%
	1-5	89038319	67	89045996	21	89666837	91	0.01%	0.71%
	1-6	130758934	563	130758934	138	131969732	342	0.00%	0.93%
	1-7	143842815	581	143842815	95	145727688	356	0.00%	1.31%
ISG2	1-8	94826436	529	94826436	83	95933439	334	0.00%	1.17%
	1-9	107811547	580	107811547	88	108700980	360	0.00%	0.82%
	1-10	121766252	605	121766252	103	122857944	348	0.00%	0.90%
	1-11	100332708	1983	100332708	324	103154925	891	0.00%	2.81%
	1-12	113063570	2206	113063570	302	114874076	773	0.00%	1.60%
ISG3	1-13	139960829	2056	139960829	302	143528487	854	0.00%	2.55%
	1-14	90906924	2005	90906924	308	93451384	821	0.00%	2.80%
	1-15	103820448	2093	103820448	271	107790446	765	0.00%	3.82%
	1-16	141124871	>3600	141124871	469	147884632	1235	0.00%	4.79%
	1-17	154254761	>3600	154254761	428	157192517	1153	0.00%	1.90%
ISG4	1-18	105673019	3542	105673019	460	111139815	1152	0.00%	5.17%
	1-19	145300515	3418	145300515	471	148278317	1271	0.00%	2.05%
	1-20	96209733	3528	96213367	461	99516349	1051	0.00%	3.44%
Avg.		117777886	1336	117778755	221	120104172	608	0.00%	1.99%

Notes: (1) 'OBJ' is the objective values in units of RMB. (2) 'Time' is the computation time in units of second (s). (3) 'Gap1' is calculated by: $(OBJ_{LR\text{-}BD} - OBJ_{CPLEX}) / OBJ_{CPLEX}$, 'Gap2' is calculated by: $(OBJ_{PSO\text{-}BD} - OBJ_{CPLEX}) / OBJ_{CPLEX}$.

Table 5: Comparison between LR-BD and PSO-BD in solving large-scale instances

Instance	ID	LR-BD		PSO-BD		Gap
		OBJ	Time(s)	OBJ	Time(s)	
(1)	(2)	(3)	(4)	(5)	(6)	((5)-(3))/(3)
ISG5	2-1	119315379	1225	125053467	1924	4.81%
	2-2	132918711	1135	143086294	1750	7.65%
	2-3	97165554	1145	103304441	2023	6.32%
	2-4	110617833	1052	118993050	1901	7.57%
	2-5	123107286	1029	129868805	2078	5.49%
ISG6	2-6	124457415	1565	139841904	2651	12.36%
	2-7	88992678	2544	102011308	2813	14.63%
	2-8	115813971	1592	130626312	2726	12.79%
	2-9	128628296	2135	141319824	2764	9.87%
	2-10	92745962	1606	108294176	2390	16.76%
Avg.		113376309	1503	124239958	2302	9.83%

***Notes**:* (1) 'OBJ' is the objective values in units of RMB. (2) 'Time' is the computation time in units of second (s). (3) 'Gap' is calculated by: $(OBJ_{PSO\text{-}BD} - OBJ_{LR\text{-}BD}) / OBJ_{LR\text{-}BD}$.

5.3. Sensitivity analysis

5.3.1. Analysis of charter in cost c_k^{zr} and charter out revenue c_k^{zc}

Figures 3 and 4 show the impact of the unit cost c_k^{zr} of chartering in a YT on the total operating cost and the number of YTs chartered. As shown in Figure 3, with the increase of unit charter in cost, the total port operation cost shows an increasing trend (the black curve), while the number of YTs chartered (the blue curve) stabilized after a small range fluctuation. The number of YTs retrofitted is not affected by c_k^{zr} (the red curve). Figure 4 shows the gap of the total cost between one value and the former value with regard to the charter in cost. The value of the gap is obviously not equal, indicating that the total cost follows a non-linear increasing trend.

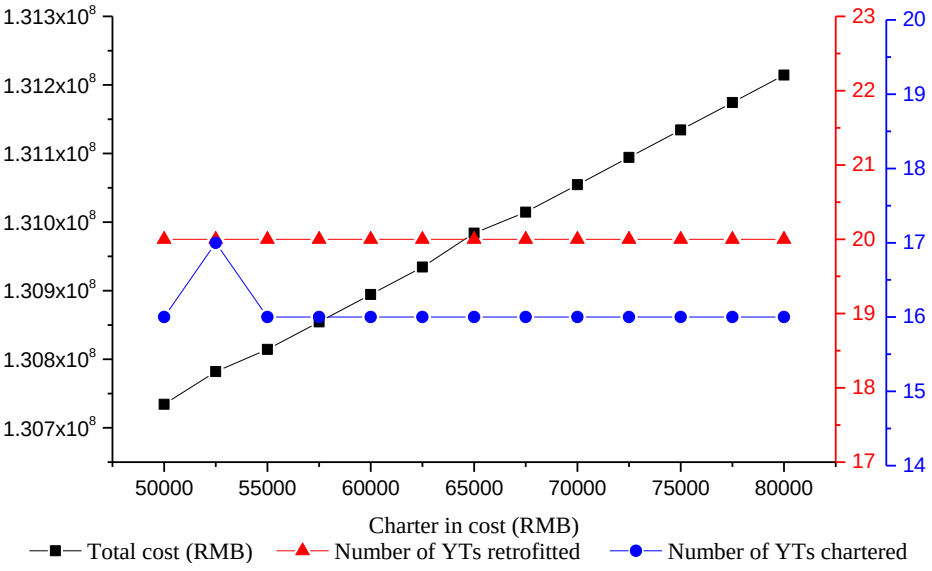

Figure 3: Analysis of charter in cost c_k^{zr}

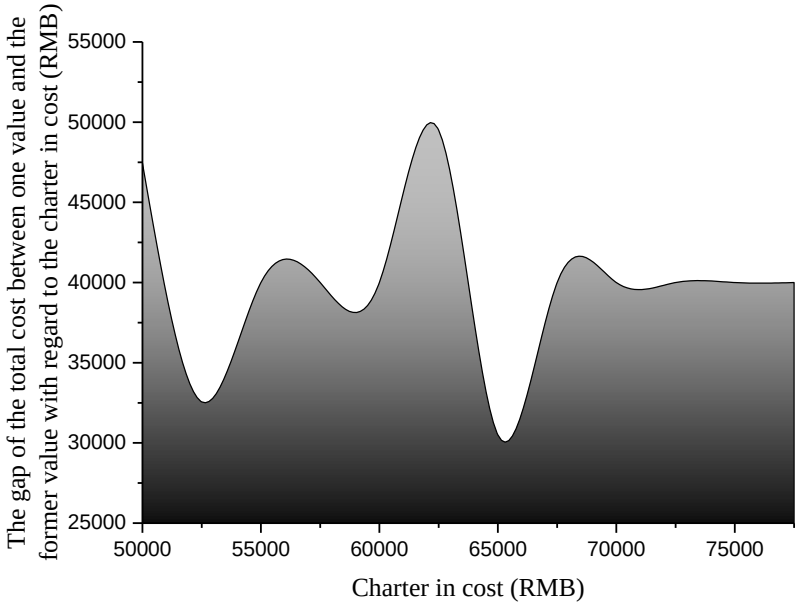

Figure 4: Total cost gap affected by charter in cost c_k^{zr}

Figures 5 and 6 show the impact of the unit income of charter out a YT c_k^{zc} on the total operating cost of the green port and the number of YTs chartered. As shown in Figure 5, with the increase of unit charter out revenue, the total cost shows a declining trend (the black curve), while the number of YTs chartered shows a stable trend at the first stage, followed by a rising trend, and then fluctuated in a small range (the blue curve). The number of YTs retrofitted decreases with charter out revenue above 34,000 RMB, and stables with charter out revenue above 36,000 RMB (the red curve). Figure 6 shows the gap of the total cost between one value and the former value with regard to the charter out revenue. The value of the gap shows curved line, that means the total cost follows a non-linear increase trend.

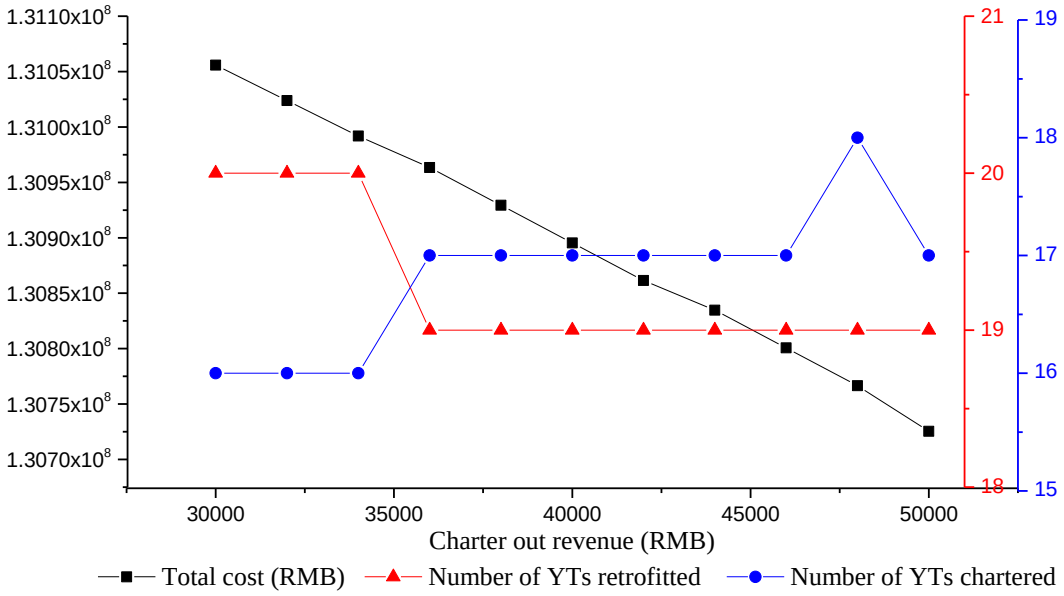

Figure 5: Analysis of charter out revenue c_k^{zc}

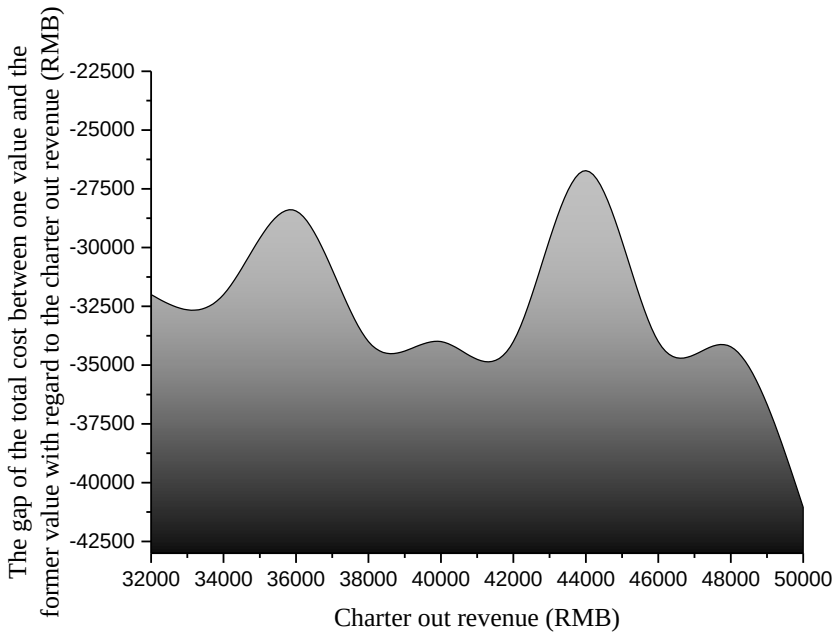

Figure 6: Total cost gap affected by charter out revenue c_k^{zc}

5.3.2. Analysis of retrofitting cost $c_{k,k'}^{v}$

Figures 7-9 show the impact of unit retrofitting cost $c_{k,k'}^{v}$ on the total cost of the green port, and the number of YTs retrofitted and chartered. As shown in Figure 7, with the increase of the unit retrofitting cost $c_{0,1}^{v}$ of manned diesel YTs to manned electric YTs, the total cost exhibits a continues rising trend (the black curve). When $c_{0,1}^{v}$ is between 60,000 and 95,000 RMB, the numbers of YTs chartered and retrofitted remains unchanged. Then the numbers fluctuate, and the sum of the numbers does not change. When the number of YTs retrofitted drops sharply, the number of shared YTs chartered rises to fill the vacancy of YTs and to ensure the smooth progress of YTs

operations. Figure 8 shows the gap of the total cost between one value and the former value with regard to the retrofitting cost $c_{0,1}^{v}$.

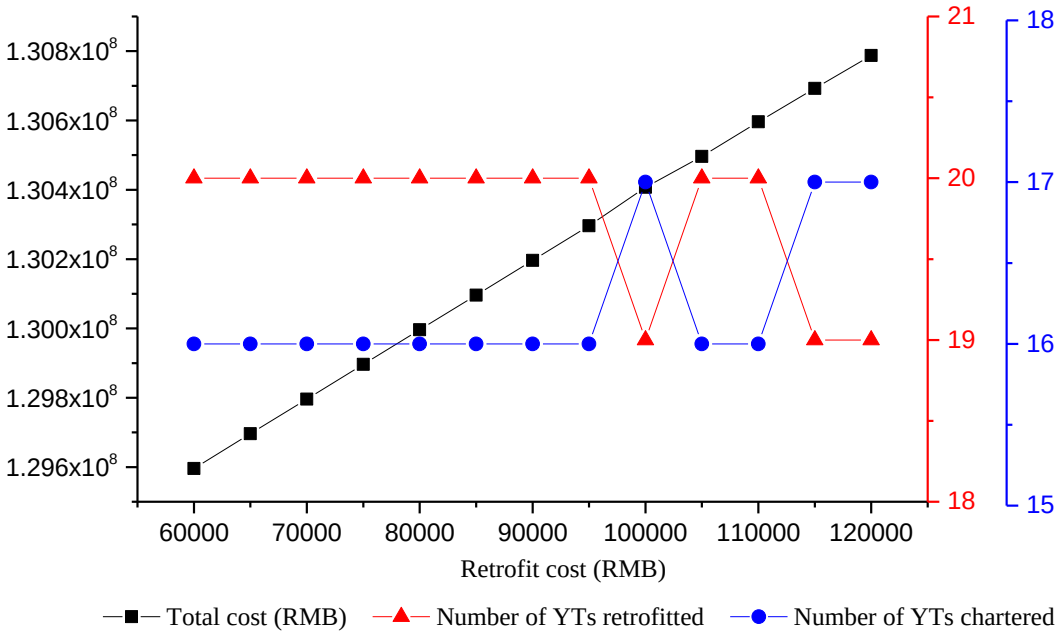

Figure 7: Analysis of retrofitting cost $c_{0,1}^{v}$

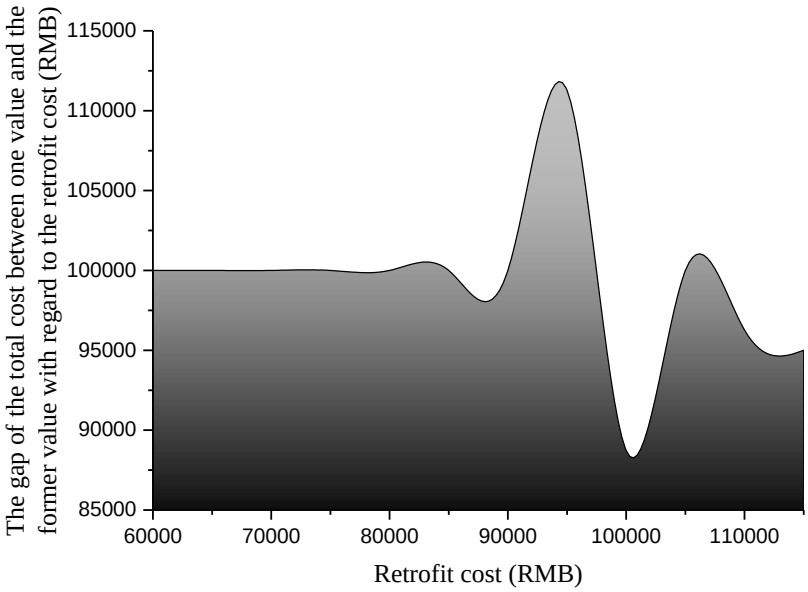

Figure 8: Total cost gap affected by retrofitting cost $c_{0,1}^{v}$

As shown in Figure 9, with the increase of unit retrofitting cost $c_{0,3}^{v}$ of manned diesel YTs to unmanned LNG YTs, the total cost and the numbers of YTs retrofitted and chartered are fluctuating. When the retrofitting cost is between 80,000 and 90,000, the total cost is minimized (the black curve). Because the change range of the unit retrofitting cost $c_{0,3}^{v}$ is close to a YT charter in cost and charter out revenue, the retrofitting cost greatly affects the number of YTs chartered. Therefore, the unit retrofitting cost $c_{0,3}^{v}$ has a significant impact on the deployment

decision of port YTs.

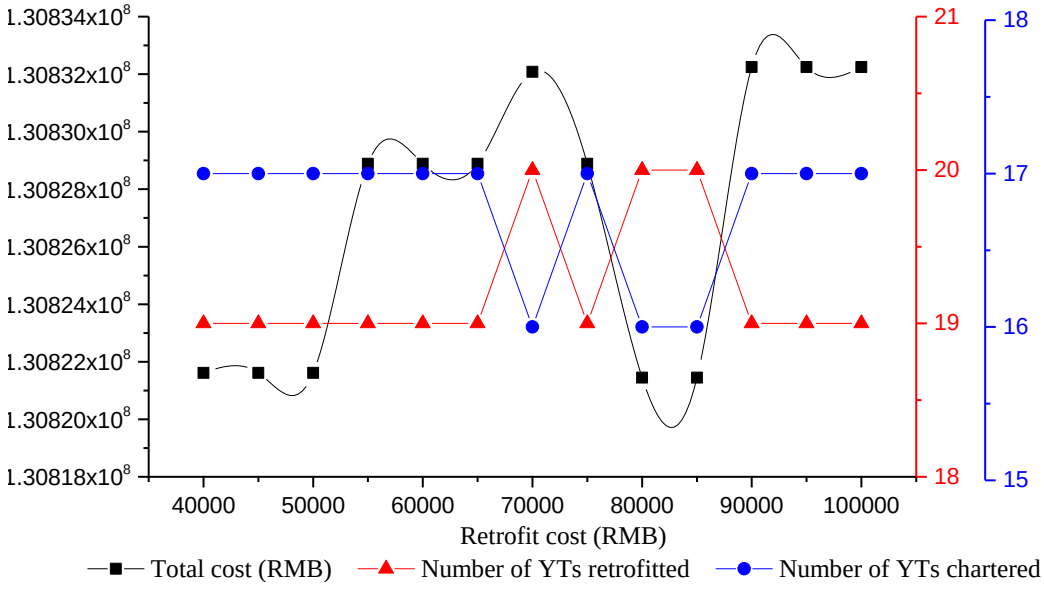

Figure 9: Analysis of retrofitting cost $c_{0,3}^{v}$

5.3.3. Analysis of Carbon emission quota E_t

The free carbon emission quota E_t does not affect the number of YTs, while slightly affects the total cost. As shown in Figure 10, with the increase of carbon emission quota, the total cost fluctuates slightly within a certain range, while the overall trend is declining. However, specific analysis is still needed. When E_t is between 200 and 400, the total cost is reduced. While when E_t is set to 700, the total operating cost of the enterprise reaches the highest value.

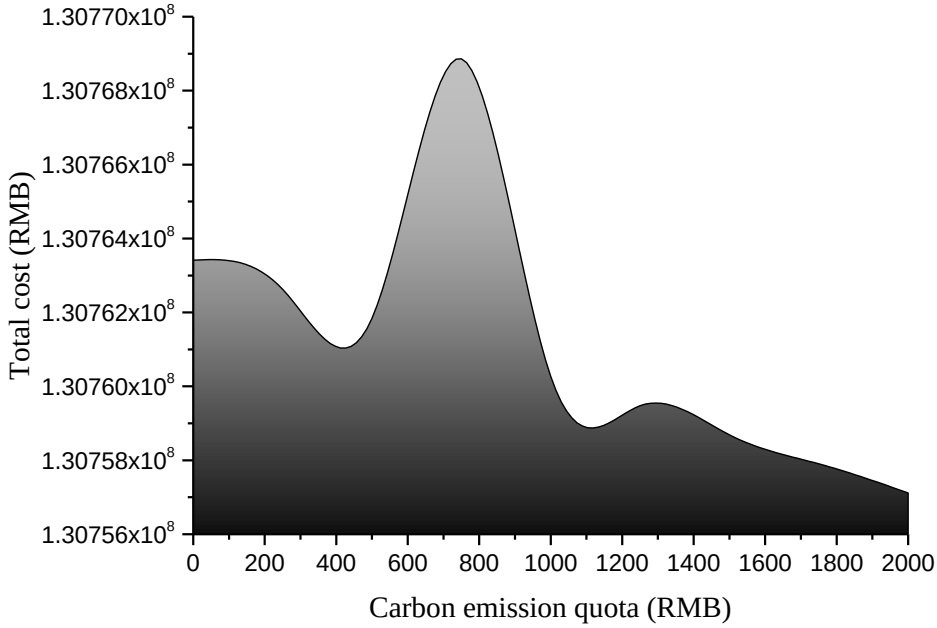

Figure 10: Analysis of carbon emission quota E_t

5.3.4. Analysis of increased workloads $h_{t,0,s}$

Figure 11 shows the impact of the increased workloads of non-hazardous materials transportation tasks $h_{t,0,s}$ on the total cost, and the numbers of YTs retrofitted, chartered in/out. With the increase of workloads, the total cost shows a linear increasing trend (the blue curve). The number of YTs retrofitted shows a trend of increase first and then stabilize (the pink curve), while the numbers of YTs chartered in/out both show a trend of decrease first, and followed by a rising trend (the green and orange curves). Figure 12 shows the gap of the total cost between one value and the former value with regard to the increased workloads $h_{t,0,s}$. It is obvious that the total cost follows a non-linear increasing trend.

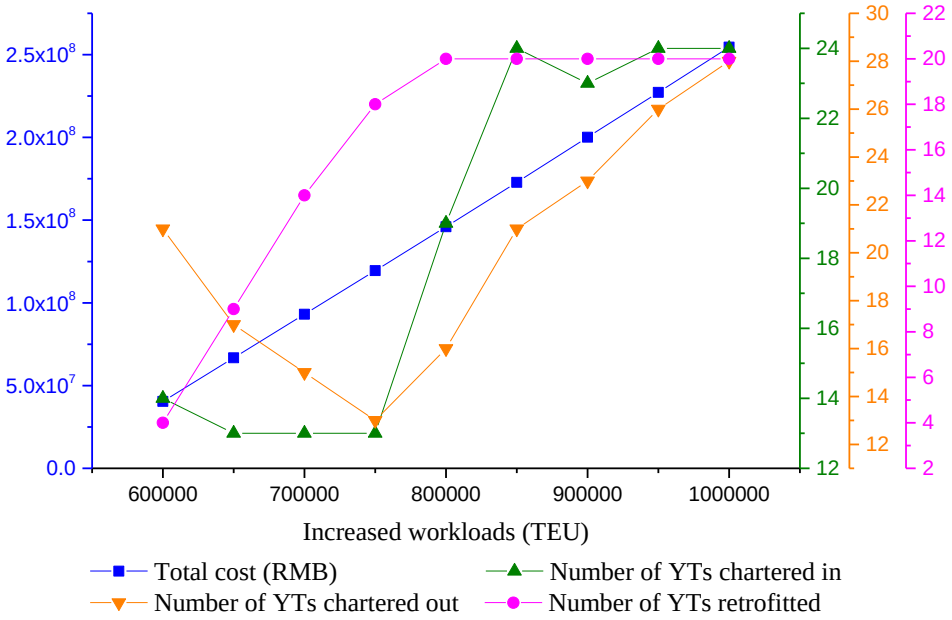

Figure 11: Analysis of the increased workloads of non-hazardous materials transportation tasks $h_{t,0,s}$

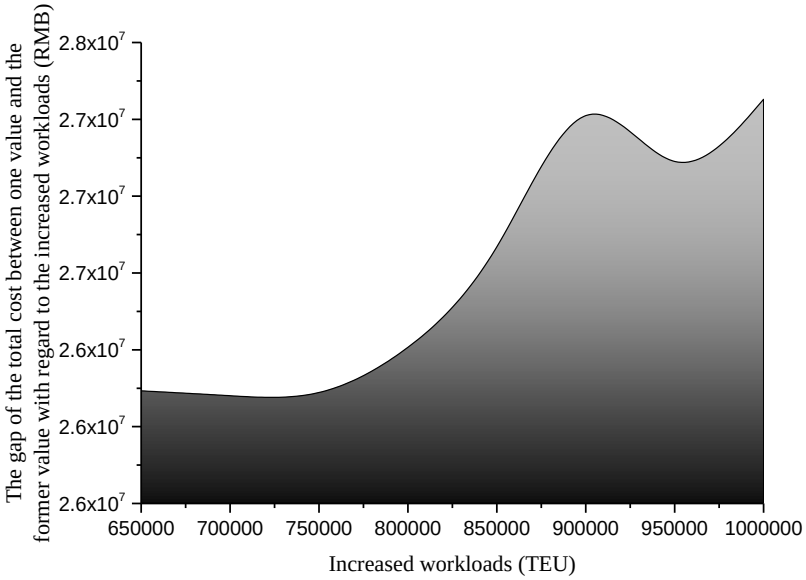

Figure 12: Total cost gap affected by the increased workloads $h_{t,0,s}$

5.4. Discussions and analysis

In this study, we analyze the charter in/out costs and retrofitting costs of YTs, the carbon emission quota, and the increased workloads in green ports, and provide the following management insights:

(1) The automation retrofitting of some yards is restricted by their conditions when mature automation technologies are applied. The laying of navigation magnetic nails is unnecessary for unmanned YTs and is more suitable for the retrofitting of traditional ports. Production operations often continue while retrofitting takes place, so the retrofit of a yard is typically divided into multiple stages.

(2) The changes in shared YTs chartered in/out, the retrofitting costs, the carbon emission quota, and the increased workloads will affect the total cost, the numbers of YTs chartered, and the retrofit. As Figures 3 to 12 show, the trends in the numbers of YTs chartered in and out are generally similar, while an opposite trend in the number of YTs retrofitted is observed. Thus, enterprises must also be aware of the status of production and retrofit during the retrofitting process, to ensure that they have sufficient equipment at each stage to maintain normal production levels.

(3) The number of retrofitted YTs does not appear to change with the increase in the charter cost of the shared YTs. The increase in the charter out revenue of YTs causes a significant uptrend of the number of YTs chartered, which peaks when the revenue reaches 47,500 RMB, and the flow of shared YTs is at its most active. The number of YTs retrofitted stabilizes after a decline when the charter out revenue is between 34,000 and 36,000 RMB.

(4) The total cost increases with the retrofitting cost $c_{0,1}^{v}$. When $c_{0,3}^{v}$ is between 80,000 and 90,000 RMB, the total operating cost of the yard can be minimized. The government subsidies provided to enterprises are based on the market value and assist enterprises when implementing low-carbon retrofitting of their yards and thus achieving the green retrofitting of the ports.

(5) As the free carbon emission quota allocated by the government to the port E_t increases, the overall operating cost of enterprises shows a downward trend. However, larger is not necessarily better, and specific port analyses are still required. In general, this can provide suggestions to the government on how to control GHG emissions and can help enterprises actively choose green technology upgrades.

6. Conclusions

This study proposes a strategic decision-making strategy for the retrofitting and deployment of YTs using a stochastic mixed-integer programming model. The strategy supports decision-makers and can inform the sustainable development of green ports. The main contributions of this study are summarized as follows.

(1) Studies of the retrofitting and deployment of YTs mainly focus on the operational level. Our proposed model considers the transportation of hazardous materials and the introduction of a shared YTs mechanism at strategic level, which have not been fully considered in the reported literatures. The model is also applicable to other allocation problems in random operation instances.

(2) As the time-steps and number of scenarios increase, CPLEX and exact solution methods find the proposed model difficult to handle. We propose enhanced Benders decomposition using a Lagrangian relaxation algorithm to solve the problem of YTs retrofitting and deployment. LR-BD can obtain the exact solution for large-scale real environments in a short time.

(3) In addition to the support given by the quantitative mathematical model to retrofitting and deployment decisions at the strategic level, we also confirm the effectiveness of the proposed model and algorithm using the real case of a port in Shanghai. Our sensitivity analysis of the various parameters can inform decision makers about the optimum approach. However, we find that increasing the free carbon emission quotas provided by the government does not necessarily lead to improvements to control GHG emissions.

However, there are limitations for the current study. This study did not consider the impact of different government emission policies on the target. Future research can optimize green ports and shipping technologies that may be adopted under emission classification policies and emission control policies (Zhen et al., 2019). In addition, other cutting plane methods can be used to accelerate the BD algorithm.

Appendix A. Algorithmic steps for enhanced Benders decomposition using Lagrangian relaxation.

Algorithm 1 Enhanced Benders decomposition using Lagrangian relaxation.

Step 1: Input: $\mathrm{UB}_{LR} = +\infty$, $\mathrm{LB}_{LR} = -\infty$, $\mathrm{UB}_{LR\_BD} = +\infty$, $\mathrm{LB}_{LR\_BD} = -\infty$,iteration number $m = 1$, tolerance error τ.

Step 2: Introduce Lagrangian multipliers $\sigma_{k,t}$ to get the Lagrangian relaxation problem $LR(\sigma)$.

Step 3: Solve the $LR(\sigma)$ to optimality, update LB_{LR}.

Step 4: Solve the Lagrangian dual problem LD along the subgradient direction, update UB_{LR}.

Step 5: Update the Lagrangian multiplier $\sigma_{k,t}^{m+1}$ of the next iteration according to constraint (56), and return to step 3.

Step 6: LR procedure stop conditions: (i) $\mathrm{UB}_{LR} = LR\left(\sigma_{k,t}^{m}\right)$, (ii) step adjustment factor $\xi^m < 0.0001$, or (iii) number of iterations $m > 100$.

Step 7: Substitute the current optimal value of each decision variable obtained by the LR into the MP of the BD to solve the solution, and obtain a better initial LB_{LR_BD}.

Step 8: Solve the dual problem and generate Pareto optimal cut according to the core point, update UB_{LR_BD}.

Step 9: Compare the gap between UB_{LR_BD} and LB_{LR_BD} with tolerance error τ, if the gap is greater than τ, update LB_{LR_BD} and continue to execute step 8, repeat until the stop conditions are reached and output the optimal solution.

Appendix B. Enhanced Benders decomposition using particle swarm optimization (PSO-BD)

Another acceleration method of BD is to combine with heuristic algorithm. Gopalakrishnan Easwaran combines Tabu Search (TS) heuristic algorithm with BD. TS provides a feasible initial upper bound for BD and a good Benders cut (Easwaran & Üster, 2009). Santoso et al. (2005) integrated sample average approximation (SAA) and BD to provide solutions for large-scale stochastic programming problems in multiple scenarios. As a widely used heuristic algorithm, PSO algorithm possesses the advantages of fast convergence speed and simple operation. In this paper, PSO is combined with BD to accelerate BD algorithm.

PSO was proposed by Eberhart and Kennedy in 1995 (Kennedy & Eberhart, 1995), which originated from the research on the predation behavior of birds, and used the sharing of information among individuals in the

population to find the optimal solution. The potential solution of the optimal problem is called "particle", and the velocity and position of the particle are continuously updated iteratively by following the optimal particle in the solution space. By introducing adaptive inertia weight and dynamically adjusting the inertia weight with the changes of iteration times and particle flight, the convergence speed can be effectively improved while balancing the global search.

(1) Initial solution generation

The quality of particle initial information has a great impact on the solution quality of meta heuristic algorithm. A better initial solution can effectively improve the solution quality of the algorithm. The steps for generating the initial solution are shown in Algorithm 2.

Algorithm 2 Initial solution generation.

Step 1 Set 0-1 variables $\omega_{k,t,l} \sim \mathrm{U}(0, w_{k,l}]$, according to constraints (12), set $\omega_{0,t,l} = 1$.

Step 2 According to constraints (1) and (2), set $\mu_{k,0}$ in the initial state.

Step 3 According to constraints (5), set $\beta_{k,k',t} = 0$ in the initial state, in the case of $t \neq 0$、$k' \neq 0$、$k \neq 2$、$k \neq 3$ and $k' \neq 3$, when $k = 1$, $\beta_{k,k',t}$ is set to a random number of $(0, \mu_{k,t-1})$, otherwise, $\beta_{g,g',a,t} = 0$.

Step 4 According to constraints (6), $\eta_{k,t}$ is set to a random number of $(0, z_{k,t})$.

Step 5 According to constraints (8), because $\varepsilon_{k,t}$ is greater than or equal to 0, judge whether $\mu_{k,t-1} - M \cdot \lambda_{t-1,l,s} \cdot w_{k,l}$ is greater than 0. If so, $\varepsilon_{k,t}$ is set to a random number of $(0, \mu_{k,t-1} - M \cdot \lambda_{t-1,l,s} \cdot w_{k,l})$. If not, set $\varepsilon_{k,t} = 0$.

Step 6 Because $\mu_{k,t-1}$ is greater than or equal to 0, judge whether $\mu_{k,t-1} + \eta_{k,t} + \sum_{k' \in K: k' \neq k} \beta_{k',k,t} - \varepsilon_{k,t} - \sum_{k' \in K: k' \neq k} \beta_{k,k',t}$ is less than 0. If so, $\gamma_{k,t}$ is set to the absolute value of $\mu_{k,t-1} + \eta_{k,t} + \sum_{k' \in K: k' \neq k} \beta_{k',k,t} - \varepsilon_{k,t} - \sum_{k' \in K: k' \neq k} \beta_{k,k',t}$. If not, set $\gamma_{k,t} = 0$.

Step 7 According to constraints (4), set $\mu_{k,t} = \mu_{k,t-1} + \gamma_{k,t} + \eta_{k,t} + \sum_{k' \in K: k' \neq k} \beta_{k',k,t} - \varepsilon_{k,t} - \sum_{k' \in K: k' \neq k} \beta_{k,k',t}$.

Step 8 According to constraints (10) and (11), $\alpha_{k,t,l}$ is set to a random number of $(0, \mu_{k,t} \cdot \omega_{k,t,l})$.

Step 9 According to constraints (18) and (19), set $\theta_{k,t,l,s} = \{0, \min(\alpha_{k,t,l} \cdot q_{k,l}, h_{t,l,s} + \lambda_{t-1,l,s})\}$. Then calculate the value of $\lambda_{t,l,s}$ from equation constraints (20) and (21). When $\lambda_{t-1,l,s} + h_{t,l,s} - \sum_{k \in K} \theta_{k,t,l,s} \leq 0$, $\lambda_{t,l,s} = 0$.

(2) Evaluation the $Pbest_j$ and $Gbest$

Take the objective function (1) as the fitness function, evaluate the fitness value of each particle, and find the

best position $Pbest_j$ experienced by the individual particle j and the best position $Gbest$ experienced by the group.

(3) Update particles

By judging the subordinate relationship between decision variables, this paper selects the variables $\omega_{k,t,l}, \mu_{k,t}, \beta_{k,k',t}, \eta_{k,t}, \varepsilon_{k,t}, \alpha_{k,t,l}$ to be updated.

$$\mathrm{V}_i^k = wV_i^{k-1} + c_1 r_1\left(Pbest_i - x_i^{k-1}\right) + c_2 r_2\left(Gbest - x_i^{k-1}\right) \tag{58}$$

$$x_i^k = x_i^{k-1} + V_i^{k-1} \tag{59}$$

Equation (58) represents the update particle velocity, and equation (59) represents the update particle position. V_i^k is the velocity vector of particle i at the kth iteration. x_i^k is the position vector of particle i at the kth iteration. w is inertia weight. c_1 and c_2 represent learning factors, which adjust the maximum step length of learning. r_1 and r_1 represent random numbers between (0,1), which increase the randomness of the search.

Select the solution with the smallest objective function value among the candidate solutions, update the current optimal solution and judge whether the maximum number of iterations is reached. If so, output the global optimal solution. If not, proceed the next iteration.

(4) PSO-BD

Substitute the $Gbest$ obtained by the PSO and the current optimal value of each decision variable into the MP of the BD to solve the solution, and return to section 4.1and 4.2 for iteration.

Reference

Abdelmagid, A., Gheith, M., & Eltawil, A. (2021). A comprehensive review of the truck appointment scheduling models and directions for future research. *Transport Reviews.* In press, doi: 10.1080/01441647.2021.1955034.

Adulyasak, Y., Cordeau, J. F., & Jans, R. (2015). Benders decomposition for production routing under demand uncertainty. *Operations Research, 63*(4), 851-867.

Anonymous. (2020). Vehicle retrofit LNG project analysis report. Accessed on August 4, 2021, from https://max.book118.com/html/2020/0423/5044210234002241.shtm.

Bailey, D., & Solomon, G. (2004). Pollution prevention at ports: clearing the air. *Environmental Impact Assessment Review, 24*(7-8), 749-774.

Benders, J. F. (1962). Partitioning procedures for solving mixed-variables programming problems. *Numerische Mathematik, 4*(1), 238–252.

Carlo, H. J., Vis, I. F. A., & Roodbergen, K. J. (2014). Transport operations in container terminals: Literature overview, trends, research directions and classification scheme. *European Journal of Operational Research, 236*(1), 1-13.

Caroe, C. C., & Tind, J. (1998). L-shaped decomposition of two-stage stochastic programs with integer recourse. *Mathematical Programming, 83*(3), 451-464.

Chen, J., Huang, T., Xie, X., Lee, P. T.-W., & Hua, C. (2019). Constructing Governance Framework of a Green and Smart Port. *Journal of Marine Science and Engineering, 7*(4), 83.

Chen, J., Zheng, H., Wei, L., Wan, Z., Ren, R., Li, J., Li, H., Bian, W., Gao, M.,& Bai, Y. (2020). Factor diagnosis and future governance of dangerous goods accidents in China's ports. *Environmental Pollution, 257*. 113582.

Chen, S. (2016). Container Terminal Carbon Emissions Accounting and Low-carbon Development Research. Master, South China University of Technology, Guangzhou, China.

Cheng, H. (2020). CO2 treatment process and equipment. Accessed on August 4, 2021, from https://www.jinchutou.com/p-132208050.html.

Cheng, H., & Jie, G. (2019). The development of green port in Shanghai Port. Accessed on August 4, 2021, from http://www.chinaports.com/portlspnews/549.

Clay, R. L., & Grossmann, I. E. (1997). A disaggregation algorithm for the optimization of stochastic planning models. *Computers & Chemical Engineering, 21*(7), 751-774.

Clott, C. B., & Hartman, B. C. (2013). Clean trucks in California ports: modelling emissions policy. *International Journal of Shipping and Transport Logistics, 5*(4-5), 449-462.

Easwaran, G., & Üster, H. (2009). Tabu search and Benders decomposition approaches for a capacitated closed-loop supply chain network design problem. *Transportation Science, 43*(3), 301-320.

Hartman, B. C., & Clott, C. B. (2012). An economic model for sustainable harbor trucking. *Transportation Research Part D-Transport and Environment, 17*(5), 354-360.

He, J., Zhang, W., Huang, Y., & Yan, W. (2013). A simulation optimization method for internal trucks sharing assignment among multiple container terminals. *Advanced Engineering Informatics, 27*(4), 598-614.

Heilig, L., Lalla-Ruiz, E., & Voss, S. (2017). Multi-objective inter-terminal truck routing. *Transportation Research Part E-Logistics and Transportation Review, 106*, 178-202.

Hervas-Peralta, M., Poveda-Reyes, S., Enrique Santarremigia, F., & Dolores Molero, G. (2020). Designing the layout of terminals with dangerous goods for safer and more secure ports and hinterlands. *Case Studies on Transport Policy, 8*(2), 300-310.

Huang, Q., Zheng, G. (2016). Route optimization for autonomous container truck based on rolling window. *International Journal of Advanced Robotic Systems*. In press, doi: 10.5772/64116.

IMO. (2021). Fourth greenhouse gas study 2020. Accessed on 23 July, 2021, from https://www.imo.org/en/OurWork/Environment/Pages/Fourth-IMO-Greenhouse-Gas-Study-2020.aspx

Iris, C., Lam, J. S. L. (2021). Optimal energy management and operations planning in seaports with smart grid while harnessing renewable energy under uncertainty. *Omega-International Journal of Management Science*. In press, doi: 10.1016/j.omega.2021.102445.

Islam, S. (2018). Simulation of truck arrival process at a seaport: evaluating truck-sharing benefits for empty trips reduction. *International Journal of Logistics-Research and Applications, 21*(1), 94-112.

Ji, S. W., Luan, D., Chen, Z. R., & Guo, D. (2021). Integrated scheduling in automated container terminals considering AGV conflict-free routing. *Transportation Letters, 13*(7), 501-513.

Jin, T., Shi, T., & Park, T. (2018). The quest for carbon-neutral industrial operations: renewable power purchase versus distributed generation. *International Journal of Production Research, 56*(17), 5723-

5735.

Kennedy, J., & Eberhart, R. (1995). Particle swarm optimization. *Proceedings of the IEEE International Conference on Neural Networks, 4*, 1942-1948.

Lee, H., Hoang Thai, P., Kim, C., & Lee, K. (2019). A study on emissions from drayage trucks in the port city-focusing on the port of incheon. *Sustainability, 11*(19). 5358.

Lu, H., & Huang, L. (2021). Optimization of shore power deployment in green ports considering government subsidies. *Sustainability, 13*(4). 1640.

Magnanti, T. L., & Wong, R. T. (1981). Accelerating Benders decomposition: algorithmic enhancement and model selection criteria. *Operations Research, 29*(3), 464-484.

Noyan, N. (2012). Risk-averse two-stage stochastic programming with an application to disaster management. *Computers & Operations Research, 39*(3), 541-559.

Noyan, N., Balcik, B., & Atakan, S. (2016). A stochastic optimization model for designing last mile relief networks. *Transportation Science, 50*(3), 1092-1113.

Qin, H., Su, X., Ren, T., & Luo, Z. (2021). A review on the electric vehicle routing problems: Variants and algorithms. *Frontiers of Engineering Management, 8*(3), 370-389.

Rahmaniani, R., Crainic, T. G., Gendreau, M., & Rei, W. (2017). The Benders decomposition algorithm: A literature review. *European Journal of Operational Research, 259*(3), 801-817.

Ramirez-Nafarrate, A., Gonzalez-Ramirez, R. G., Smith, N. R., Guerra-Olivares, R., & Voss, S. (2017). Impact on yard efficiency of a truck appointment system for a port terminal. *Annals of Operations Research, 258*(2), 195-216.

Rowangould, D., Rowangould, G., & Niemeier, D. (2018). Evaluation of the health impacts of rolling back a port clean trucks program. *Transportation Research Record, 2672*(11), 53-64.

Saharidis, G. K. D., & Konstantzos, G. E. (2018). Critical overview of emission calculation models in order to evaluate their potential use in estimation of Greenhouse Gas emissions from in port truck operations. *Journal of Cleaner Production, 185*, 1024-1031.

Santoso, T., Ahmed, S., Goetschalckx, M., & Shapiro, A. (2005). A stochastic programming approach for supply chain network design under uncertainty. *European Journal of Operational Research, 167*(1), 96-115.

Schulte, F., Lalla-Ruiz, E., Gonzalez-Ramirez, R. G., & Voss, S. (2017). Reducing port-related empty truck emissions: A mathematical approach for truck appointments with collaboration. *Transportation Research Part E-Logistics and Transportation Review, 105*, 195-212.

Seddiek, I. S. (2020). Application of renewable energy technologies for eco-friendly sea ports. *Ships and Offshore Structures, 15*(9), 953-962.

Steenken, D., Voss, S., & Stahlbock, R. (2004). Container terminal operation and operations research - a classification and literature review. *OR Spectrum, 26*(1), 3-49.

Tan, Z., Zhang, Q., Yuan, Y., & Jin, Y. (2021). A decision method on yard cranes transformation and deployment in green ports. *International Transactions in Operational Research, 29*(1), 323-346.

UNCTAD. (2018). Review of Maritime Transport 2018. Accessed on 23 July, 2021, from https://unctad.org/system/files/official-document/rmt2018_en.pdf

UNCTAD. (2020). Review of Maritime Transport 2020. Accessed on 23 July, 2021, from https://unctad.org/system/files/official-document/rmt2020_en.pdf

Vis, I. F. A., & de Koster, R. (2003). Transshipment of containers at a container terminal: An overview. *European Journal of Operational Research, 147*(1), 1-16.

Wang, K., & Jacquillat, A. (2020). A stochastic integer programming approach to air traffic scheduling and operations. *Operations Research, 68*(5), 1375-1402.

Wang, S., Zhen, L., & Psaraftis, H. (2021). Three potential benefits of the EU and IMO's landmark efforts to monitor carbon dioxide emissions from shipping. *Frontiers of Engineering Management, 8*(2), 310-311.

Wang, T., Wang, X., & Meng, Q. (2018). Joint berth allocation and quay crane assignment under different carbon taxation policies. *Transportation Research Part B-Methodological, 117*, 18-36.

Wang, Z. X., Chan, F. T. S., Chung, S. H., & Niu, B. (2014). A decision support method for internal truck employment. *Industrial Management & Data Systems, 114*(9), 1378-1395.

Watson, F. R., & Rogers, D. F. (2007). Pareto-optimality of the Balinski cut for the uncapacitated facility location problem. *International Journal of Operations Research, 4*(3), 155-164.

Xin, J. B., Negenborn, R. R., Corman, F., & Lodewijks, G. (2015). Control of interacting machines in automated container terminals using a sequential planning approach for collision avoidance. *Transportation Research Part C-Emerging Technologies, 60*, 377-396.

Kaluarachchi, Y. (2021). Potential advantages in combining smart and green infrastructure over silo approaches for future cities. *Frontiers of Engineering Management, 8*(1), 98-108.

Zhang, H., Zhang, Q., & Chen, W. (2019). Bi-level programming model of truck congestion pricing at container terminals. *Journal of Ambient Intelligence and Humanized Computing, 10*(1), 385-394.

Zhang, J., Ioannou, P. A., & Chassiakos, A. (2006). Automated container transport system between inland port and terminals. *ACM Transactions on Modeling and Computer Simulation, 16*(2), 95-118.

Zhang, X., Zeng, Q., & Yang, Z. (2019). Optimization of truck appointments in container terminals. *Maritime Economics & Logistics, 21*(1), 125-145.

Zhen, L. (2017). A bi-objective model on multiperiod green supply chain network design. *IEEE Transactions on Systems, Man, and Cybernetics: Systems, 50*(3), 771-784.

Zhen, L., Zhuge, D., Murong, L., Yan, R., & Wang, S. (2019). Operation management of green ports and shipping networks: overview and research opportunities. *Frontiers of Engineering Management, 6*(2), 152-162.

Zhong, H., Hu, Z., & Yip, T. L. (2019). Carbon emissions reduction in China's container terminals: optimal strategy formulation and the influence of carbon emissions trading. *Journal of Cleaner Production, 219*, 518-530.

Zhou, D., Ding, H., Wang, Q., & Su, B. (2021). Literature review on renewable energy development and China's roadmap. *Frontiers of Engineering Management, 8*(2), 212-222.